DUAL FREQUENCY BROADBAND MICROSTRIP AN-TENNA WITH A REACTIVE LOADING AND STACKED ELEMENTS

J. Anguera [†], C. Puente[‡], and C. Borja

Technology and Intellectual Property Rights Department
Fractus, Barcelona, Spain

Abstract—A dual-band enhanced-bandwidth microstrip antenna is presented with a frequency separation of $f_2/f_1 = 1.33$. In order to achieve the dual-frequency operation, a rectangular patch is loaded with a stub at one of its radiating edges. To improve bandwidth at each band, two parasitic patches are coupled to the driven element.

1. INTRODUCTION

Microstrip antennas are good antenna candidates when certain directivity is needed such as base station applications. One of the main challenges is to achieve an acceptable bandwidth for multi-band operation. A vast work has been done in this field [1–7] however most of the research has been focused in narrow band solutions. In [7–10], authors present dual-band broadband techniques having different frequency ratios. In [11], the bandwidth of a dual-band patch antenna using a reactive load is improved using a dual-band parasitic element. Although, such a technique offered a satisfactory bandwidth enhancement, the radiation pattern at the second band was tilted (not pointing to the broadside direction). In some applications such as base stations antennas, a critical specification is to obtain a broadside beam. Therefore in this paper, the research done in [11] has been improved replacing the former dual-band element by two parasitic elements coupled to the driven element. Each parasitic operates in its fundamental mode and it is responsible of enhancing the radiation at each band. Many other techniques may be found in the literature for

---

Corresponding author: J. Anguera (jaume.anguera@fractus.com).
[†] Also with Electronics and Communications, Universitat Ramon Llull, Barcelona, Spain.
[‡] Also with Signal Theory and Communications, Universitat Politècnica de Catalunya, Barcelona, Spain.

dual-band behavior [12, 13] but the main purpose here is to concentrate of a particular case using a driven element close the groundplane (1.52 mm). This is an advantage when the element is integrated in an array environment since the feeding networks and the antenna feeding element can be printed in the same conductive layer. This simplifies the mechanics of the antennas which is very critical for base station arrays.

2. RESULTS

To circumvent the radiation pattern distortion of the solution presented in [11], a technique based on two stacked parasitic elements is used. The driven patch is etched on a substrate of $120 \times 120 \, \text{mm}^2$ where the groundplane is etched on the bottom part. This groundplane is also
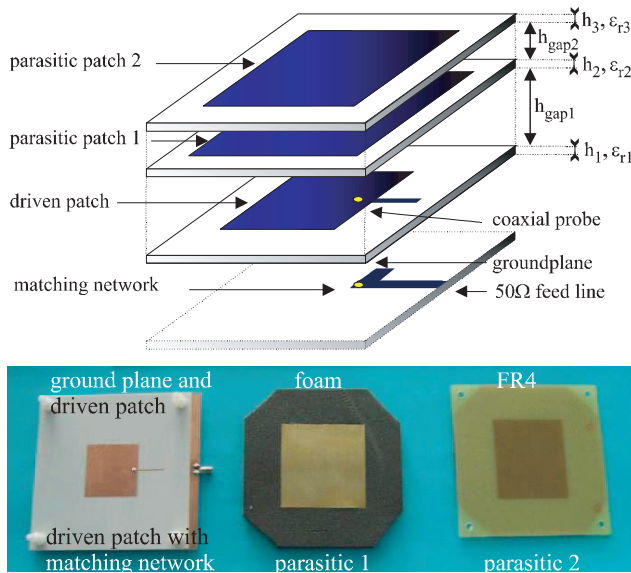

Figure 1. Experimental dimensions. Driven patch: 40×40, $h_1 = 1.52$, $\varepsilon_{r1} = 3.38$, reactive loaded with a stub of length 20 and thickness 0.5; Parasitic element 1: 63×63, $h_2 = 1$, $\varepsilon_{r2} = 1.03$; Parasitic element 2: 59×59, $h_3 = 1$ and $\varepsilon_{r3} = 1.03$; $h_{gap1} = 9$, $h_{gap2} = 1$. Groundplane is 120×120. An extra layer of FR4 1 mm thick is placed on the top parasitic patch acting as a parasitic support and as a radome. The centers are aligned. All dimensions in mm. Feeding point 17 mm from the edge where the stub (10.2 mm length, 6.6 mm width) is placed.

the groundplane for the feeding microstrip line and matching network. The microstrip line is fed using an SMA connector. The parasitic patch 1 is made of brass 0.2 mm thick and placed on a foam substrate 1 mm thick. The parasitic patch 2 is etched on the bottom part of a FR4 substrate 1 mm thick.

Bandwidth is optimized by carefully choosing the resonant frequencies of the parasitic elements and the coupling between them and the driven patch.

To adjust the parasitic patch size, the distance between the driven and the parasitic elements and the position of the feeding point, the iterative process presented in [14] to design stacked antennas is followed. Such process is applied for both parasitic elements. The electrical model shown in Fig. 2 represents the dual-mode patch antenna modeled by two series RLC resonators having different resonant frequencies. Each parasitic model is also modeled by RLC resonators which are coupled to the driven element. Parasitic element 1 having a resonant frequency f_{p1} is coupled to the driven element RLC at f_{d1}. If both resonant frequencies are the same, an input impedance loop appears at the real axis of the Smith chart. The size of such a loop is controlled by the coupling between the distance of the parasitic element and the driven element which is represented by C_{c1}. The same applies for the second resonance, that is, f_{d2} and f_{p2}. For the second
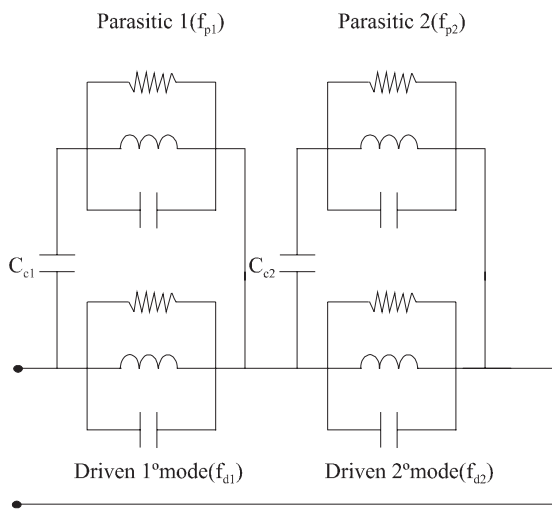

Figure 2. Electrical model for the dual-mode antenna. C_{c1} and C_{c2} take into account the coupling between each parasitic element and the driven patch.

resonance, the coupling is modeled by C_{c2}. This model has been also used to understand the dual-band behavior of a fractal-based Sierpinski microstrip patch antenna [10, 15]. The process can be summarized as follows [10], (c) 2004, IEEE.

- The input impedance loop can be controlled by properly choosing the feeding point on the driven patch in the overcoupled zone of the Smith chart (Z_i at resonance > $Z_o = 50\,\Omega$ (reference impedance). For stacked structures in order to have the input impedance loop centered at the Smith chart, the input impedance on the driven patch when the parasitic patch is not present, must be greater than $Z_o = 50\,\Omega$ because the parasitic patch shifts the input impedance to lower values.

- The input impedance loop will be inductive if $f_p < f_d$ and vice versa being f_p and f_d the parasitic patch and driven patch resonance frequencies respectively. This comment is useful because on can adjust the input impedance loop position by changing the feeding point and by adjusting the resonant frequency of the parasitic patch. That is, the feeding point moves the input impedance loop in a horizontal path on the Smith chart while the relation between resonant frequencies moves the input impedance loop in a vertical path (capacitive or inductive zone of the Smith chart).

- The input impedance loop size increases as the coupling between the driven and parasitic patches increases. Coupling increases as the gap between driven and parasitic patches decreases. Therefore, depending of the specified SWR, one can separate more or less the gap between patches in order to inscribe the input impedance loop on the circle of constant SWR.

According to [14], to place the impedance loops in the centre of the Smith chart, a high impedance feeding point is required. Since there are two loops, a feeding point that allows matching in both bands at the same time is quite difficult in spite of the fact that two parasitic patches are used. Therefore, a simple matching network (transmission line + stub) is used to centre the impedance loops inside the circle of SWR = 2 (Fig. 3(a)). Fig. 3(a) shows one band centered at 1.743 GHz having a bandwidth of 14.9% (1.9 GHz and 16.2% predicted, respectively), and a second one centered at 2.318 GHz with a bandwidth of 2.36% (2.391 GHz and 2.43% predicted, respectively).

The measured resonance frequencies are lower than predicted (using IE3D MoM package), whereas the measured bandwidths are quite similar to the predicted ones. The bandwidth enhancement factor F (ratio between the bandwidth for this solution and the one obtained

(a)   (b)
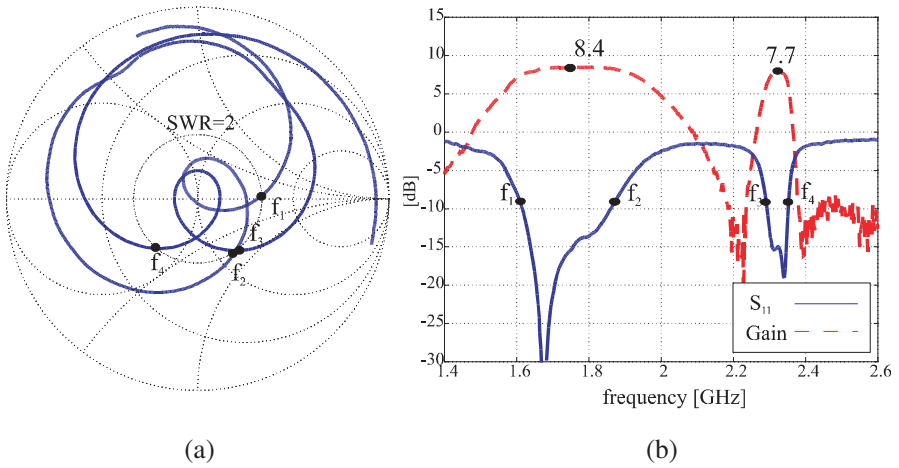
Figure 3. (a) Measured input impedance: $f_1 = 1.619\,\text{GHz}$, $f_2 = 1.874\,\text{GHz}$, $f_3 = 2.298\,\text{GHz}$ and $f_4 = 2.353\,\text{GHz}$. (b) Measured reflection coefficient and gain. Gain has been measured in the direction $\theta = 0°$ corresponding to the co-polarized gain. The cross-polarized gain is under $-30\,\text{dB}$.
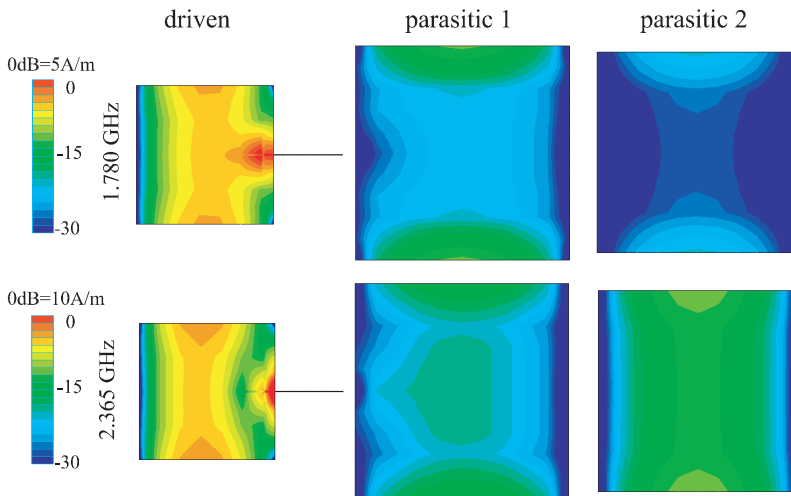

Figure 4. Simulated electrical current on the patch surfaces. It can be observed that parasitic patches have a fundamental mode current distribution.

with the driven element only) is 9 for the first band and 5 for the second one: the bandwidth has been enhanced satisfactorily.

Antenna gain is measured in the direction in which it is supposed to be maximum ($\theta = 0°$ in the simulation). The measured gain is 8.4 dB (9.0 dB predicted) in the first band and 7.7 dB (9.2 dB predicted) in the second one, as seen in Fig. 3(b). The gain is kept constant along both bands, dropping 0.97 dB with regard to the first extreme frequency (f_1) and 0.12 dB with regard to the second (f_2) one in the first band. In the second band, it drops 1.64 dB with regard to the first extreme frequency (f_3) and 1.7 dB with regard to the second one (f_4).

In order to study in greater depth the physical behavior of this structure, the electrical current on the patch surfaces is computed to know which parasitic patch contributes to radiation at each operating band. Fig. 4 shows the electrical current distribution on the patch surface at 1.780 and 2.365 GHz where it can be observed that for the first operating band only the largest parasitic patch seems to contribute to radiation while the other is transparent. However, for the second operating frequency, both parasitic patches contribute to radiation. The main difference between these current distributions and those for one parasitic solution [11] is that the parasitic patches, in the present case, show the current distribution of the fundamental mode. This effect is transferred into the radiation pattern where the problem of beam-tilting of the previous solution has now successfully disappeared (Fig. 5, Fig. 6).
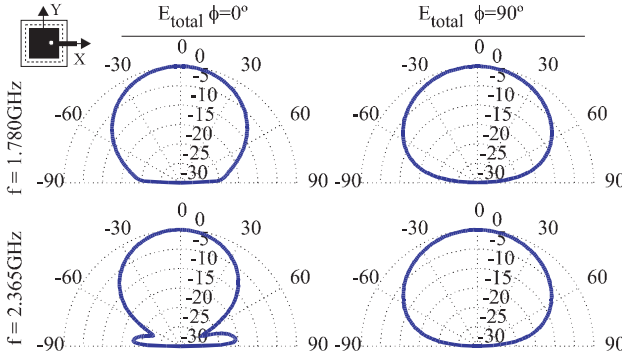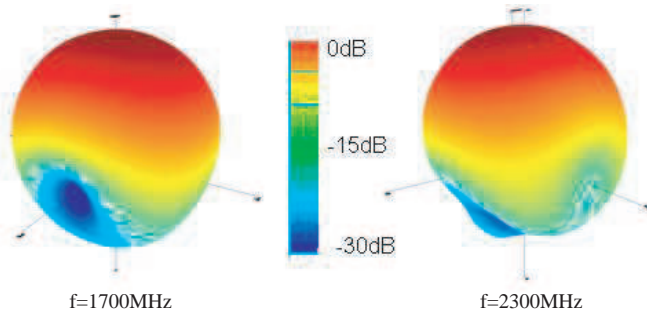

Figure 5. Simulated main radiation cuts considering an infinite groundplane.

Measured radiation patterns are calculated for $f = 1.700$ GHz and $f = 2.300$ GHz where it can be observed that both frequencies present a broadside radiation pattern (Fig. 6); the correction of the tilting of the pattern can be observed here compared to the one shown in [11]. This

$$\varphi = 0^{\circ} \qquad \varphi = 90^{\circ}$$

Frequency = 1700MHz

Frequency = 2300MHz
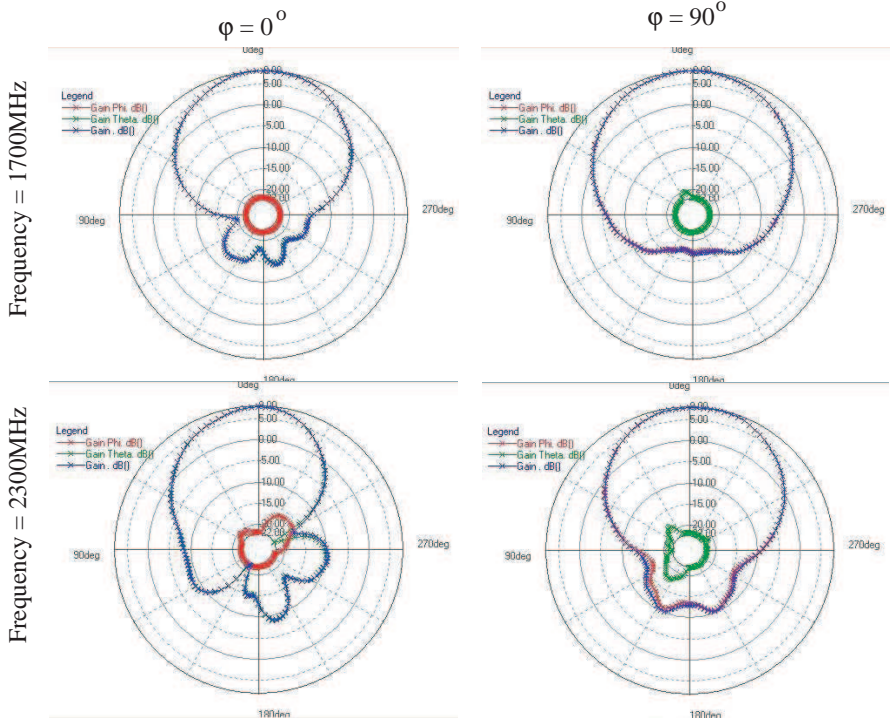
Figure 6. Measured radiation cuts for E ($\varphi = 90°$) and H planes ($\varphi = 0°$).

f=1700MHz   f=2300MHz

Figure 7. 3D normalized measured radiation patterns. Dynamic range is 30 dB.

is the advantage of the present technique using two parasitic patches with respect to the previous one using only one where the radiation pattern for the second band was slightly tilted. In this case, however, the bandwidth for the 2nd has been reduced.

Table 1. Summary of the main measured parameters.

	$f = 1700\,\text{MHz}$	$f = 2300\,\text{MHz}$
$\Delta\theta_{-3\,\text{dB}}$ E-plane [°]	76.8	68.7
$\Delta\theta_{-3\,\text{dB}}$ H-plane [°]	62.3	52.3
Directivity [dB]	8.5	9.3
Worst XPD across $\Delta\theta_{-3\,\text{dB}}$ E-plane [dB]	> 26	> 25
Worst XPD across $\Delta\theta_{-3\,\text{dB}}$ H-plane [dB]	> 28	> 24
Front to back ratio [dB]	21	16

Finally, to obtain all the radiation parameters, a full 3D measurement has been done using the Satimo StarGate-32 anechoic chamber at Fractus-lab (Fig. 7). The main antenna parameters are summarized in Table 1.

3. CONCLUSION

In this paper, a way to obtain a dual-band antenna with enhanced bandwidths from a dual-band narrow-band antenna has been presented.

The enhancement factors have been proved to be 9 in the first band and 5 in the second one, achieving bandwidths of 14.9% and 2.36% respectively. With regard to the gain, it is 8.4 dB in the first band and 7.7 dB in the second one; radiation patterns are both broadside which is of particular interest of base station antennas. The main disadvantage is the reduced bandwidth obtained in the second band compared to the solution presented in [11].

REFERENCES

1. Maci, S. and G. Biffi Gentili, "Dual frequency patch antennas," *IEEE Antennas and Propag. Magazine*, Vol. 39, No. 6, December 1997.

2. Lee, C. S., V. Nalbandian, and F. Schwering, "Planar dualband microstrip antenna," *IEEE Trans. Antennas Propag.*, Vol. 43, No. 8, 892–894, August 1995.

3. Daniel, A. E. and G. Kumar, "Tuneable dual and triple stub loaded," *IEEE Trans. Antennas Propag.*, Vol. 48, No. 7, 1026–1039, July 2000.

4. Wang, B. F. and Y. T. Lo, "Microstrip antennas for dual-frequency operation," *IEEE Trans. Antennas Propag.*, Vol. 32, 938–943, September 1984.

5. Anguera, J., G. Font, C. Puente, C. Borja, and J. Soler, "Multifrequency microstrip patch antenna using multiple stacked elements," *IEEE Microwave and Wireless Component Letters*, Vol. 13, No. 3, March 2003.

6. Wang, Y. J. and C. K. Lee, "Design of dual-frequency microstrip patch antennas and application for IMT-2000 mobile handsets," *Progress In Electromagnetics Research*, PIER 36, 265–278, 2002.

7. Luk, K. M., C. H. Lai, and K. F. Lee, "Wideband L-probe-fed patch antenna with dualband operation for GSM/PCS base stations," *Electron. Lett.*, Vol. 35, 1123–1124, July 1999.

8. Tang, C. L., C. W. Chiou, and K. L. Wong, "Broadband dual-frequency V-shape patch antenna," *Microwave Opt. Technol. Lett.*, Vol. 25, 121–123, April 2000.

9. Anguera, J., C. Puente, C. Borja, N. Delbene, and J. Soler, "Dual frequency broadband stacked microstrip patch antenna," *IEEE Antennas and Wireless Propag. Letters*, Vol. 2, 36–39, 2003.

10. Anguera, J., E. Martínez, C. Puente, C. Borja, and J. Soler, "Broadband dual-frequency microstrip patch antenna with modified Sierpinski fractal geometry," *IEEE Trans. Antennas Propag.*, Vol. 52, No. 1, 66–73, January 2004.

11. Anguera, J., C. Puente, C. Borja, and J. Soler, "Dual-frequency broadband-stacked microstrip antenna using a reactive loading and a fractal-shaped radiating edge," *IEEE Antennas and Wireless Propag. Letters*, Vol. 6, 309–312, 2007.

12. Wong, K. L., *Compact and Broadband Microstrip Antennas, Wiley Series in Microwave and Optical Engineering*, Chapter 4, 2002.

13. Kumar, G. and K. P. Ray, *Broadband Microstrip Antennas*, Chapter 7, Artech House, 2003.

14. Anguera, J., C. Puente, and C. Borja, "Procedure to design electromagnetically coupled microstrip patch antennas based on a simple network model," *Microwave Opt. Technol. Lett.*, Vol. 30, No. 3, 149–151, August 2001.

15. Anguera, J., "Fractal and broadband techniques on miniature, multifrequency, and high-directivity microstrip patch antennas," Ph.D. Dissertation at the Dept. of Signal Theory and Communications, Universitat Politècnica de Catalunya, 2003.